

***CP* violation in chargino decays in the MSSM**

Wei Min Yang* and Dong Sheng Du

*CCAST(World Laboratory), P.O.Box 8730, Beijing 100080, China and
Institute of High Energy Physics, P.O.Box 918(4), Beijing 100039, China*

ABSTRACT

In the minimal supersymmetric standard model (MSSM) with complex parameters, supersymmetric loop effects can lead to *CP* violation. We calculate the rate asymmetries of decays of charginos into the lightest neutralino and a *W* boson on the basis of the most important loop contributions in the third generation squark sectors. It turns out that the *CP* violating asymmetries can be a few per cent in typical regions of the parameter space of the MSSM. These processes would provide very promising channels for probing *CP* violation in the MSSM at future high-energy colliders.

PACS numbers: 12.60.Jv, 13.90.+i, 14.80.Ly

*Email address: yangwm@mail.ihep.ac.cn

I. INTRODUCTION

Searching for new CP violating effects beyond the standard model (SM), is an important and interesting work for theoretical and experimental high-energy physicist. The MSSM are currently considered as the most theoretically well motivated extensions of the (SM) [1, 2]. In comparison with the sole CKM phase in the SM, it contains more diverse sources of CP violation through complex soft-SUSY-breaking parameters [3]. These new soft phases affect not only CP violating observables but can have significant impacts in a variety of places [4], including $g_\mu - 2$, electric dipole moments (EDMs), CP violation in the K and B systems, the baryon asymmetry of the universe, cold dark matter, superpartner production cross sections and branching ratios, and rare decays. Although there are some experiments that suggest some of the phases are small, mainly the neutron and electron EDMs [5], it has recently been realized that CP violating phases associated with the third generation trilinear soft-breaking terms might be large and can induce sizable CP violation in the Higgs and the third generation sfermion sectors through loop corrections [6, 7]. Such phases may allow baryogenesis and do not necessarily violate the stringent bound from the nonobservation of (EDMs) [8]. In fact, some of these phases can be $\mathcal{O}(1)$, so as to provide non-SM sources of CP violation required for dynamical generation of the baryon asymmetry of the universe [9, 10]. The important implication of the CP violating phases in the search for supersymmetry has received growing attention.

The decays of charginos $\tilde{\chi}_i^+$ ($i = 1, 2$) and neutralinos $\tilde{\chi}_l^0$ ($l = 1 - 4$) in the MSSM under CP conservation have been extensively studied [11]. For most of the parameter space of the MSSM, the decays of the heaviest chargino $\tilde{\chi}_2^+$ and the two heavier neutralinos $\tilde{\chi}_l^0$ ($l = 3, 4$) will be dominated by two-body tree-level processes in which the final states include two possible classes: (i) a lighter neutralino or chargino plus a W , Z , or Higgs boson; and (ii) channels involving squarks or sleptons if they are kinematically allowed. For the lightest chargino $\tilde{\chi}_1^+$ and the next lightest neutralino $\tilde{\chi}_2^0$, the mass difference between them and the lightest neutralino $\tilde{\chi}_1^0$ is not usually so large, therefore their dominant decay modes are three-body tree-level decays through a virtual vector boson or Higgs boson mediation. But in some parameter region, the mass splitting between them can exceed the mass of a vector boson or Higgs boson, in this case, the type (i) will be the most important decay modes of them. Furthermore, if they are enough heavy, the decay channels of the type (ii) are also possible. In fact, the above decays can also occur at one-loop level via the final state interactions if they are kinematically accessible, furthermore, the CP violating phases can directly affect the couplings of charginos and neutralinos to the third generation sfermions. Therefore,

the interferences of the tree diagrams of these decays with the corresponding one-loop diagrams can make their partial decay widths difference from that of corresponding CP conjugate processes. In this paper, as an example, we will focus on CP violation in the decays of charginos into the lightest neutralino and a W boson as the two-body-decay branching ratios can be large. It can be measured by the rate asymmetry:

$$A_{cp} = \frac{\Gamma(\tilde{\chi}_i^+ \rightarrow \tilde{\chi}_1^0 W^+) - \Gamma(\tilde{\chi}_i^- \rightarrow \tilde{\chi}_1^0 W^-)}{\Gamma(\tilde{\chi}_i^+ \rightarrow \tilde{\chi}_1^0 W^+) + \Gamma(\tilde{\chi}_i^- \rightarrow \tilde{\chi}_1^0 W^-)}. \quad (1)$$

Of course, analogous asymmetries can also be discussed for the other decay channels of charginos and neutralinos.

The remainder of this paper is organized as follows: in Section II we list the relevant couplings and give the analytical formulas of the decay rate asymmetries. In Sec.III, we present detailed numerical results. Our conclusions are summarized in Sec.IV. Appendix A outlines the necessary masses and mixing matrices, and appendix B contains the expressions of the form factors.

II. RELEVANT COUPLINGS AND DECAY RATE ASYMMETRY

In order to calculate the rate asymmetry of decays of charginos into the lightest neutralino and a W boson, in the appendix A we review briefly the masses and mixing of the chargino, neutralino and sfermion sectors of the MSSM. As mentioned in last section, although the tree-level decays of charginos is invariant under CP , a nonvanishing value of the rate asymmetry A_{cp} in Eq. (1) is generated at one-loop level by complex couplings. Among others, the most significant CP violating effects arise from the trilinear couplings of the third generation $A_{t,b,\tau}$ [12], especially from squark sectors because of the Yukawa characteristic factor m_q (m_q is the mass of quark q) in the chargino/neutralino-quark-squark couplings. Therefore, one can expect that the most important contributions come from one-loop quark-squark exchange diagrams, as shown in Fig. 1 (a-d). The relevant interaction Lagrangian are listed as follows [1]:

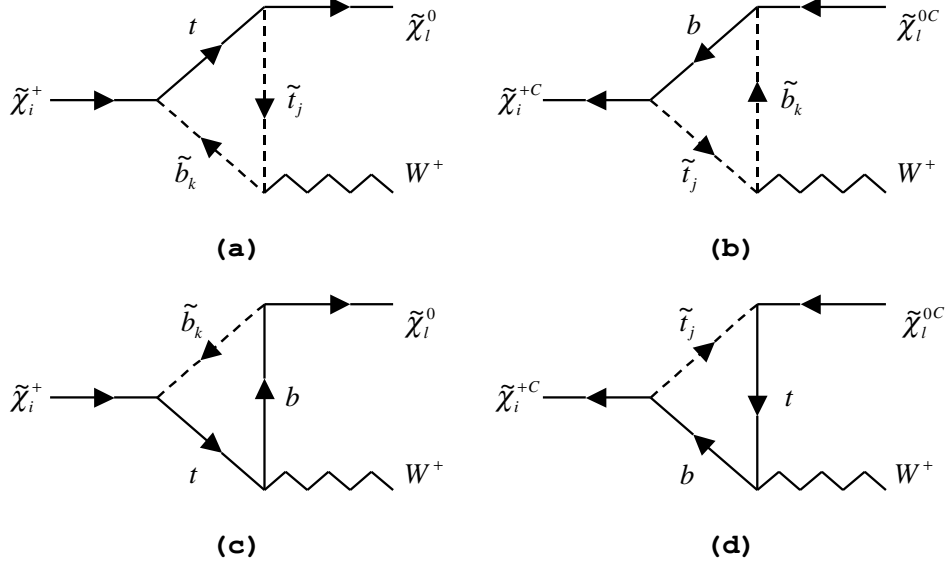


FIG. 1. The relevant one-loop diagrams for the decay $\tilde{\chi}_i^+ \rightarrow \tilde{\chi}_l^0 W^+$.

$$\begin{aligned}
\mathcal{L}_{\tilde{\chi}^+ q \tilde{q}'} &= \bar{t}(A_{ik}^L P_L + A_{ik}^R P_R) \tilde{\chi}_i^+ \tilde{b}_k + \bar{b}(B_{ij}^L P_L + B_{ij}^R P_R) \tilde{\chi}_i^{+c} \tilde{t}_j \\
&\quad + \overline{\tilde{\chi}_i^+} (A_{ik}^{R*} P_L + A_{ik}^{L*} P_R) \tilde{t} \tilde{b}_k^* + \overline{\tilde{\chi}_i^{+c}} (B_{ij}^{R*} P_L + B_{ij}^{L*} P_R) \tilde{b} \tilde{t}_j^*, \\
\mathcal{L}_{\tilde{\chi}^0 q \tilde{q}} &= \bar{t}(C_{lj}^L P_L + C_{lj}^R P_R) \tilde{\chi}_l^0 \tilde{t}_j + \bar{b}(D_{lk}^L P_L + D_{lk}^R P_R) \tilde{\chi}_l^0 \tilde{b}_k \\
&\quad + \overline{\tilde{\chi}_l^0} (C_{lj}^{R*} P_L + C_{lj}^{L*} P_R) \tilde{t} \tilde{t}_j^* + \overline{\tilde{\chi}_l^0} (D_{lk}^{R*} P_L + D_{lk}^{L*} P_R) \tilde{b} \tilde{b}_k^*, \\
\mathcal{L}_{W \tilde{\chi}^0 \tilde{\chi}^+} &= W_\mu^- \overline{\tilde{\chi}_l^0} \gamma^\mu (E_{il}^L P_L + E_{il}^R P_R) \tilde{\chi}_i^+ + W_\mu^+ \overline{\tilde{\chi}_i^+} \gamma^\mu (E_{il}^{L*} P_L + E_{il}^{R*} P_R) \tilde{\chi}_l^0, \\
\mathcal{L}_{W \tilde{q} \tilde{q}'} &= i(F_{kj} W_\mu^- \tilde{b}_k^* \overleftrightarrow{\partial}_\mu \tilde{t}_j + F_{kj}^* W_\mu^+ \tilde{t}_j^* \overleftrightarrow{\partial}_\mu \tilde{b}_k), \\
\mathcal{L}_{W q q'} &= -\frac{g}{\sqrt{2}} (W_\mu^- \bar{b} \gamma^\mu P_L t + W_\mu^+ \bar{t} \gamma^\mu P_L b), \tag{2}
\end{aligned}$$

where $j, k = (1, 2)$, and $P_{L,R} = (1 \mp \gamma^5)/2$. The corresponding coupling

coefficients are given by

$$\begin{aligned}
A_{ik}^L &= \frac{gm_t}{\sqrt{2}m_W s_\beta} V_{i2}^* R_{k1}^{\tilde{b}*}, & A_{ik}^R &= \frac{g}{\sqrt{2}} \left[\frac{m_b}{m_W c_\beta} U_{i2} R_{k2}^{\tilde{b}*} - \sqrt{2} U_{i1} R_{k1}^{\tilde{b}*} \right], \\
B_{ij}^L &= \frac{gm_b}{\sqrt{2}m_W c_\beta} U_{i2}^* R_{j1}^{\tilde{t}*}, & B_{ij}^R &= \frac{g}{\sqrt{2}} \left[\frac{m_t}{m_W s_\beta} V_{i2} R_{j2}^{\tilde{t}*} - \sqrt{2} V_{i1} R_{j1}^{\tilde{t}*} \right], \\
C_{lj}^L &= \frac{g}{\sqrt{2}} \left[-\frac{m_t}{m_W s_\beta} N_{l4}^* R_{j1}^{\tilde{t}*} + \frac{4}{3} \tan \theta_W N_{l1}^* R_{j2}^{\tilde{t}*} \right], \\
C_{lj}^R &= \frac{g}{\sqrt{2}} \left[-\frac{m_t}{m_W s_\beta} N_{l4} R_{j2}^{\tilde{t}*} - (N_{l2} + \frac{1}{3} \tan \theta_W N_{l1}) R_{j1}^{\tilde{t}*} \right], \\
D_{lk}^L &= \frac{g}{\sqrt{2}} \left[-\frac{m_b}{m_W c_\beta} N_{l3}^* R_{k1}^{\tilde{b}*} - \frac{2}{3} \tan \theta_W N_{l1}^* R_{k2}^{\tilde{b}*} \right], \\
D_{lk}^R &= \frac{g}{\sqrt{2}} \left[-\frac{m_b}{m_W c_\beta} N_{l3} R_{k2}^{\tilde{b}*} + (N_{l2} - \frac{1}{3} \tan \theta_W N_{l1}) R_{k1}^{\tilde{b}*} \right], \\
E_{il}^L &= \frac{g}{\sqrt{2}} (\sqrt{2} V_{i1}^* N_{l2} - V_{i2}^* N_{l4}), & E_{il}^R &= \frac{g}{\sqrt{2}} (\sqrt{2} U_{i1} N_{l2}^* + U_{i2} N_{l3}^*), \\
F_{kj} &= -\frac{g}{\sqrt{2}} R_{k1}^{\tilde{b}} R_{j1}^{\tilde{t}*}.
\end{aligned} \tag{3}$$

The total amplitude of the $\tilde{\chi}_i^\pm \rightarrow \tilde{\chi}_1^0 W^\pm$ processes can be written as

$$\mathcal{M}(\tilde{\chi}_i^\pm \rightarrow \tilde{\chi}_1^0 W^\pm) = \mathcal{M}_{Tree}^{(\pm)} + \mathcal{M}_{Loop}^{(\pm)} \tag{4}$$

with

$$\begin{aligned}
\mathcal{M}_{Tree}^{(+)} &= \bar{u}_{\tilde{\chi}_1^0}(k_1) \gamma^\mu (E_{i1}^L P_L + E_{i1}^R P_R) u_{\tilde{\chi}_i^+}(p) \epsilon_\mu(k_2), \\
\mathcal{M}_{Tree}^{(-)} &= \bar{v}_{\tilde{\chi}_i^+}(-p) \gamma^\mu (E_{i1}^{L*} P_L + E_{i1}^{R*} P_R) v_{\tilde{\chi}_1^0}(-k_1) \epsilon_\mu^*(-k_2), \\
\mathcal{M}_{Loop}^{(+)} &= \bar{u}_{\tilde{\chi}_1^0}(k_1) [(\gamma^\mu \Lambda_{(+i1)}^L + p^\mu \Pi_{(+i1)}^L) P_L \\
&\quad + (\gamma^\mu \Lambda_{(+i1)}^R + p^\mu \Pi_{(+i1)}^R) P_R] u_{\tilde{\chi}_i^+}(p) \epsilon_\mu(k_2), \\
\mathcal{M}_{Loop}^{(-)} &= \bar{v}_{\tilde{\chi}_i^+}(-p) [(\gamma^\mu \Lambda_{(-i1)}^L + p^\mu \Pi_{(-i1)}^R) P_L \\
&\quad + (\gamma^\mu \Lambda_{(-i1)}^R + p^\mu \Pi_{(-i1)}^L) P_R] v_{\tilde{\chi}_1^0}(-k_1) \epsilon_\mu^*(-k_2),
\end{aligned} \tag{5}$$

where $\Lambda_{(\pm)}^{L,R}$ and $\Pi_{(\pm)}^{L,R}$ represent the form factors of vertex corrections contributed by the one-loop diagrams in Fig. 1, whose expressions are listed in the appendix B. At next-to-leading order, the CP violating asymmetry of Eq. 1 can be obtained as

$$A_{cp} = \frac{2\rho \text{Re} \delta G - 12m_{\tilde{\chi}_i^+} m_{\tilde{\chi}_1^0}^2 m_W^2 \text{Re} \delta H + \lambda(m_{\tilde{\chi}_1^0} \text{Re} \delta I + m_{\tilde{\chi}_i^+} \text{Re} \delta J)}{2\rho(|E_{i1}^L|^2 + |E_{i1}^R|^2) - 24m_{\tilde{\chi}_i^+} m_{\tilde{\chi}_1^0}^2 m_W^2 \text{Re}(E_{i1}^L E_{i1}^{R*})} \tag{6}$$

with

$$\begin{aligned}\rho &= m_W^2(m_{\tilde{\chi}_i^+}^2 + m_{\tilde{\chi}_1^0}^2 - 2m_W^2) + (m_{\tilde{\chi}_i^+}^2 - m_{\tilde{\chi}_1^0}^2)^2, \\ \lambda &= m_{\tilde{\chi}_i^+}^2 + m_{\tilde{\chi}_1^0}^2 + m_W^2 - 2m_{\tilde{\chi}_i^+}m_{\tilde{\chi}_1^0} - 2m_{\tilde{\chi}_i^+}m_W - 2m_{\tilde{\chi}_1^0}m_W,\end{aligned}\quad (7)$$

and

$$\begin{aligned}\delta G &= (\Lambda_{(+i1)}^L E_{i1}^{L*} + \Lambda_{(+i1)}^R E_{i1}^{R*}) - (\Lambda_{(-i1)}^L E_{i1}^L + \Lambda_{(-i1)}^R E_{i1}^R), \\ \delta H &= (\Lambda_{(+i1)}^L E_{i1}^{R*} + \Lambda_{(+i1)}^R E_{i1}^{L*}) - (\Lambda_{(-i1)}^L E_{i1}^R + \Lambda_{(-i1)}^R E_{i1}^L), \\ \delta I &= (\Pi_{(+i1)}^L E_{i1}^{L*} + \Pi_{(+i1)}^R E_{i1}^{R*}) - (\Pi_{(-i1)}^L E_{i1}^L + \Pi_{(-i1)}^R E_{i1}^R), \\ \delta J &= (\Pi_{(+i1)}^L E_{i1}^{R*} + \Pi_{(+i1)}^R E_{i1}^{L*}) - (\Pi_{(-i1)}^L E_{i1}^R + \Pi_{(-i1)}^R E_{i1}^L).\end{aligned}\quad (8)$$

From Eq. (6)-(8), it can directly be seen that there is no CP violation at tree level because of all of the form factors vanishing. However, for generating CP violation loop corrections, *viz.* nonvanishing form factors, and complex couplings, *viz.* nonvanishing CP violating phases, are essential factors.

III. NUMERICAL RESULTS

In this section, we will illustrate numerical results of the CP violating asymmetry based on the MSSM parameter space at the electroweak scale allowed by present data constrains [13]. In order not to vary too many parameters, we assume the grand unified theory relation for the gaugino mass parameters, $M_1 \approx 0.5M_2$. In this case, the phase of the gaugino sector can be rotated away. In addition, since the phase of Higgs mixing parameter, φ_μ , is highly constrained by the EDMs of electron and neutron [5], we take $\varphi_\mu = 0$. For the mass parameters of the squark sectors, we fix simply the relations: $M_{\tilde{U}} : M_{\tilde{Q}} : M_{\tilde{D}} \approx 0.85 : 1 : 1.05$. Thus, in our following numerical analyses the input parameters contain only: $M_2, M_{\tilde{Q}}, |\mu|, |A_t|, |A_b|, \varphi_t, \varphi_b$ and $\tan\beta$. Corresponding to a set of representative values in the parameter space as follows:

$$\begin{aligned}M_2 &= 250 \text{ GeV}, \quad M_{\tilde{Q}} = 450 \text{ GeV}, \quad |\mu| = 500 \text{ GeV}, \\ |A_t| &= |A_b| = 500 \text{ GeV}, \quad \varphi_t = \varphi_b = \frac{\pi}{4}, \quad \tan\beta = 5 \text{ or } 40,\end{aligned}\quad (9)$$

Table 1 list explicitly the relevant sparticle masses. It can be seen that because of the large Yukawa couplings of the third generation squarks, the mixing between stops or sbottoms can be very strong, especially for the case of the high value of $\tan\beta = 40$. Moreover, the masses of $\tilde{\chi}_1^0$ and $\tilde{\chi}_1^+$ approximate to the values of M_1 and M_2 , respectively, while the mass of $\tilde{\chi}_2^+$

$\tan \beta$	$m_{\tilde{\chi}_1^+}$	$m_{\tilde{\chi}_2^+}$	$m_{\tilde{\chi}_1^0}$	$m_{\tilde{t}_1}$	$m_{\tilde{t}_2}$	$m_{\tilde{b}_1}$	$m_{\tilde{b}_2}$
5	236	519	122	350	532	449	477
40	241	517	124	336	541	361	548

Table 1. The relevant sparticle masses (in GeV) for parameter sets in Eq. (9).

is about the value of $|\mu|$. In fact, this is generic in the region $|\mu| \geq M_2$ [11]. Therefore, if only M_2 and $|\mu|$ are not too low, both $\tilde{\chi}_1^\pm \rightarrow \tilde{\chi}_1^0 W^\pm$ and $\tilde{\chi}_2^\pm \rightarrow \tilde{\chi}_1^0 W^\pm$ are kinematically allowed.

We now consider only the $\tilde{\chi}_2^\pm \rightarrow \tilde{\chi}_1^0 W^\pm$ channel, and demonstrate in turn the dependence of its CP violating asymmetry A_{cp} on various choices of the parameters. Because our results are not sensitive to M_2 , it will be fixed. In Fig. 2, Absolute value of the CP asymmetry, $|A_{cp}|$, is shown as a function of the Higgs mixing parameter $|\mu|$. The four curves in this figure are corresponding to four combined choices of $\tan \beta = 5$ (or 40) and $\varphi_t = \varphi_b = \pi/4$ (or $\pi/2$), respectively. The other parameters are fixed by Eq. (9). From these curves, for instance, for the short-dashed line of $\tan \beta = 5$ and $\varphi_t = \varphi_b = \pi/4$, one can distinguish the thresholds of $b\tilde{t}_1$ at $|\mu| \approx 295$ GeV, $b\tilde{t}_2$ at $|\mu| \approx 495$ GeV, $t\tilde{b}_1$ at $|\mu| \approx 610$ GeV, $t\tilde{b}_2$ at $|\mu| \approx 650$ GeV. In the region of small $|\mu|$, the contributions to $|A_{cp}|$ come from the stop-bottom-bottom loop of Fig. 2 (b) and the stop-bottom-top loop of Fig. 2 (d). As can be seen, once $m_{\tilde{\chi}_2^+} > m_b + m_{\tilde{t}_1}$, $|A_{cp}|$ can sharply go up to order of 10^{-3} (10^{-2}) for $\tan \beta = 5$ ($\tan \beta = 40$). As the value of $|\mu|$ increasing, the $\tilde{\chi}_2^+ \rightarrow b\tilde{t}_2$ channel is open, $|A_{cp}|$ can further rise to several per cent for whether $\tan \beta = 5$ or $\tan \beta = 40$. For larger $|\mu|$, it should however be taken into account that the contributions of diagram (a) and (c) in Fig. 2 though they are relatively smaller.

In Fig. 3, we plot $|A_{cp}|$ as a function of the left-handed soft-SUSY-breaking squark mass $M_{\tilde{Q}}$ for the same arrangement of $\tan \beta$ and φ_t, φ_b as in Fig. 2. The other parameters are still given by Eq. (9). Here it is more clearly visible that the threshold of $b\tilde{t}_2$ is at $M_{\tilde{Q}} \approx 455$ (470) GeV for $\tan \beta = 5$ and $\varphi_t = \varphi_b = \pi/4$ ($\pi/2$), and at $M_{\tilde{Q}} \approx 460$ (465) GeV for $\tan \beta = 40$ and $\varphi_t = \varphi_b = \pi/4$ ($\pi/2$). For $\tan \beta = 40$, $|A_{cp}|$ is essentially of the order of 10^{-2} in the region $M_{\tilde{Q}} = 300 \sim 600$ GeV. For $\tan \beta = 5$, in the lighter squark region, namely above the threshold of $\tilde{\chi}_2^+ \rightarrow b\tilde{t}_2$, $|A_{cp}|$ is also of the order of 10^{-2} ; in the heavier squark region, the $\tilde{\chi}_2^+ \rightarrow b\tilde{t}_2$ channel is close, $|A_{cp}|$ lower to order of 10^{-3} .

The CP asymmetry as a function of the trilinear coupling $|A_t| = |A_b|$ is illustrated in Fig. 4. Here we take $|\mu| = 550$ GeV, the other parameters are still fixed by Eq. (9) and the choices of $\tan \beta, \varphi_t, \varphi_b$ are as same as the

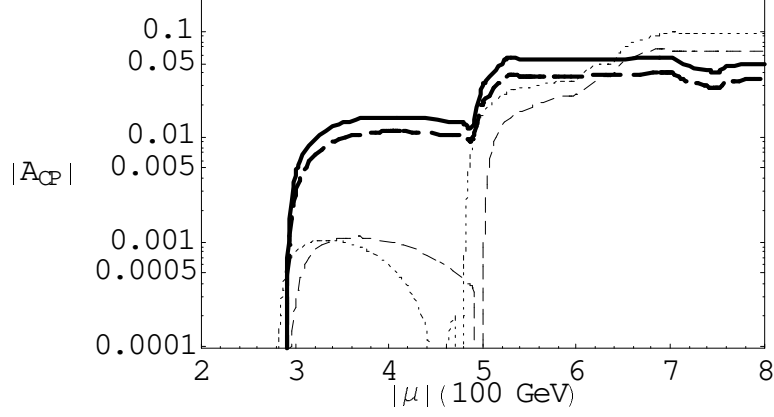


FIG. 2. Absolute value of A_{cp} as a function of $|\mu|$. The thinner short-dashed line (dotted line) is for $\tan \beta = 5, \varphi_t = \varphi_b = \pi/4$ ($\pi/2$), while the thicker long-dashed line (solid line) is for $\tan \beta = 40, \varphi_t = \varphi_b = \pi/4$ ($\pi/2$), respectively. The other parameters are fixed by Eq. (9).

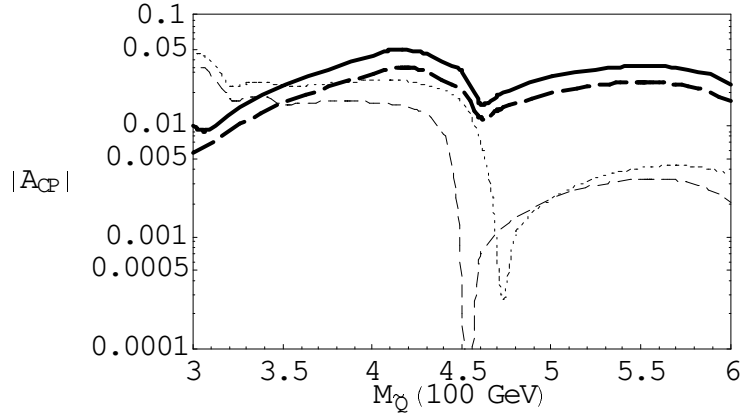


FIG. 3. $|A_{cp}|$ as a function of $M_{\tilde{Q}}$. The thinner short-dashed line (dotted line) is for $\tan \beta = 5, \varphi_t = \varphi_b = \pi/4$ ($\pi/2$), while the thicker long-dashed line (solid line) is for $\tan \beta = 40, \varphi_t = \varphi_b = \pi/4$ ($\pi/2$), respectively. The other parameters are fixed by Eq. (9).

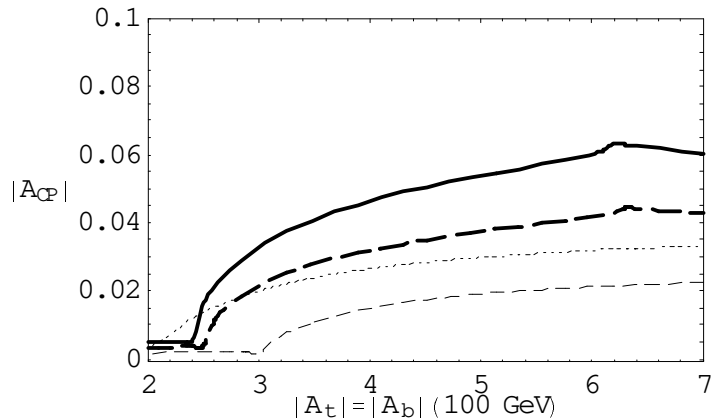


FIG. 4. $|A_{cp}|$ as a function of $|A_t| = |A_b|$ for $|\mu| = 550$ GeV. The thinner short-dashed line (dotted line) is for $\tan\beta = 5, \varphi_t = \varphi_b = \pi/4$ ($\pi/2$), while the thicker long-dashed line (solid line) is for $\tan\beta = 40, \varphi_t = \varphi_b = \pi/4$ ($\pi/2$), respectively. The other parameters are fixed by Eq. (9).

previous. For the smaller values of $|A_t| = |A_b|$, $|A_{cp}|$ is very small and below $\mathcal{O}(0.01)$. As $|A_t| = |A_b|$ increase from small to large, $|A_{cp}|$ rise to a few per cent. On the other hand, changing $\tan\beta = 5$ to $\tan\beta = 40$, the values of $|A_{cp}|$ are raised two per cent or so; varying $\varphi_t = \varphi_b$ from $\pi/4$ to $\pi/2$, $|A_{cp}|$ is enhanced about 0.01.

Fig. 5 shows the dependence of A_{cp} on the CP violating phase φ_t for the four combined choices of $\tan\beta = 5/40$ and $\varphi_b = 0/\varphi_t$. Here we take $|\mu| = 600$ GeV and $M_{\tilde{Q}} = 400$ GeV, the other parameters are given by Eq. (9). As expected, A_{cp} shows a $\sim \sin\varphi_t$ dependence. For the case of $\tan\beta = 5$, because the value of $|\mu|$ is relatively larger to the value of $M_{\tilde{Q}}$, all of the $b\tilde{t}_{1,2}, \tilde{t}b_{1,2}$ channels are open. At the two maximal stop phases, $\varphi_t = \pi/2, 3\pi/2$, the CP asymmetry can reach 6%. In this case, because the mixing between sbottoms is not so large, the influence of the phase φ_b is relatively smaller. For the case of $\tan\beta = 40$, however, the mixing between sbottoms is comparable with the mixing between stops, φ_b can obviously change A_{cp} by up to 40% at $\varphi_t = \pi/2, 3\pi/2$.

IV. CONCLUSIONS

In this work, we have discuss the possible CP violation in the decays of charginos and neutralinos in the MSSM. For the decay of the heaviest chargino into the lightest neutralino and a W boson, we have explicitly presented analytical and numerical results of the CP violating asymmetry. The decay rate asymmetry originates from the large CP violating phases

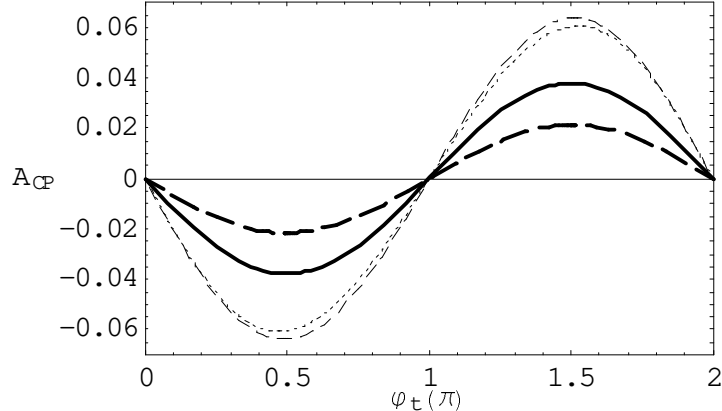


FIG. 5. A_{cp} as a function of φ_t for $M_{\tilde{Q}} = 400$ GeV and $|\mu| = 600$ GeV. The thinner short-dashed line (dotted line) is for $\tan\beta = 5, \varphi_b = 0$ (φ_t), while the thicker long-dashed line (solid line) is for $\tan\beta = 40, \varphi_b = 0$ (φ_t), respectively. The other parameters are fixed by Eq. (9).

and one-loop corrections of the third generation squark sectors. The CP asymmetry can typically reach several per cent, depending mainly on the phases and $\tan\beta$. For a larger mixing between the stops (sbottoms), the CP asymmetry is in particular evident. At a future e^+e^- linear collider with $\sqrt{s} = 500 \sim 1000$ GeV [14], the cross section of chargino pair production is around $\mathcal{O}(1)$ pb [15]. With a luminosity $\mathcal{L} = 100 \text{ fb}^{-1}$, about several hundred signal events can be expected since the decay channels has a larger branching ratio and a cleaner final signal. Therefore, Analyzing these final states would allow to measure the important couplings of squark sectors and determine the CP violating phases. Thus providing a opportunity for detecting directly the CP violating effects of the MSSM.

ACKNOWLEDGMENTS

One of the authors, W. M. Yang, thanks M. Z. Yang for helpful discussions. This work is in part supported by National Natural Science Foundation of China.

APPENDIX A: SUSY PARTICLES MASSES AND MIXING

To fix our notation, we simply summarize in this appendix the masses and mixing of the relevant sparticles. The mass matrices of charginos and neutralinos are respectively given by

$$M_C = \begin{pmatrix} M_2 & \sqrt{2}m_W s_\beta \\ \sqrt{2}m_W c_\beta & \mu \end{pmatrix} \quad (10)$$

and

$$M_N = \begin{pmatrix} M_1 & 0 & -m_Z s_W c_\beta & m_Z s_W s_\beta \\ 0 & M_2 & m_Z c_W c_\beta & -m_Z c_W s_\beta \\ -m_Z s_W c_\beta & m_Z c_W c_\beta & 0 & -\mu \\ m_Z s_W s_\beta & -m_Z c_W s_\beta & -\mu & 0 \end{pmatrix}, \quad (11)$$

where we have used the abbreviations: $s_W = \sin \theta_W$, $c_\beta = \cos \beta$, etc. M_1 and M_2 are the soft-SUSY-breaking gaugino mass parameters. μ is the Higgs mixing parameter. $\tan \beta$ is the ratio of the two Higgs vacuum expectation values. μ and one of M_i ($i = 1, 2$) can be complex. The chargino mass matrix can be diagonalized by two unitary matrices U and V ,

$$U^* M_C V^\dagger = \text{diag}(m_{\tilde{\chi}_1^+}, m_{\tilde{\chi}_2^+}), \quad (12)$$

where $m_{\tilde{\chi}_{1,2}^+}$ are the masses of the physical chargino states. The neutralino mass matrix can be diagonalized by a single unitary matrix N ,

$$N^* M_N N^\dagger = \text{diag}(m_{\tilde{\chi}_1^0}, m_{\tilde{\chi}_2^0}, m_{\tilde{\chi}_3^0}, m_{\tilde{\chi}_4^0}), \quad (13)$$

where $m_{\tilde{\chi}_l^0}$ ($l = 1 - 4$) are the masses of the physical neutralino states. The expressions of mass eigenvalues and mixing matrix elements for charginos and neutralinos can be found in Ref [11].

The mass-squared matrices of stops and sbottoms in the left-right basis can be written as

$$M_q^2 = \begin{pmatrix} m_{LL}^2 & m_{LR}^2 \\ m_{LR}^{2*} & m_{RR}^2 \end{pmatrix} \quad (q = t/b) \quad (14)$$

with

$$\begin{aligned} m_{LL}^2 &= M_{\tilde{Q}}^2 + m_q^2 + m_Z^2 \cos 2\beta (T_3^q - Q_q s_W^2), \\ m_{RR}^2 &= M_{\tilde{U}/\tilde{D}}^2 + m_q^2 + m_Z^2 \cos 2\beta Q_q s_W^2, \\ m_{LR}^2 &= m_q (A_q^* - \mu \cot \beta) / m_q (A_q^* - \mu \tan \beta), \end{aligned} \quad (15)$$

where $M_{\tilde{Q}}$ and $M_{\tilde{U}} (M_{\tilde{D}})$ are the left- and right-handed soft-SUSY-breaking stop (sbottom) masses, respectively. The soft-SUSY-breaking trilinear couplings A_q are complex parameters,

$$A_t = |A_t| e^{i\varphi_t}, \quad A_b = |A_b| e^{i\varphi_b} \quad (16)$$

with CP violating phases φ_t and φ_b . The mass-squared matrix M_q^2 can be diagonalized by a unitary matrix $R^{\tilde{q}}$,

$$R^{\tilde{q}} M_q^2 R^{\tilde{q}\dagger} = \text{diag}(m_{q_1}^2, m_{q_2}^2), \quad (17)$$

where the diagonalization matrix can be parameterized as

$$R^{\tilde{q}} = \begin{pmatrix} \cos \theta_q & \sin \theta_q e^{i\delta_q} \\ -\sin \theta_q e^{-i\delta_q} & \cos \theta_q \end{pmatrix} \quad (18)$$

with

$$\delta_t = \arg(A_t^* - \mu \cot \beta), \quad \delta_b = \arg(A_b^* - \mu \tan \beta). \quad (19)$$

The squark mass eigenvalues and mixing angle are then given as

$$m_{\tilde{q}_{1,2}}^2 = \frac{1}{2} \left[m_{LL}^2 + m_{RR}^2 \mp \sqrt{(m_{LL}^2 - m_{RR}^2)^2 + 4|m_{LR}^2|^2} \right],$$

$$\tan \theta_q = \frac{2|m_{LR}^2|}{m_{LL}^2 - m_{RR}^2 + m_{\tilde{q}_1}^2 - m_{\tilde{q}_2}^2}. \quad (20)$$

APPENDIX B: THE RELEVANT FORM FACTORS

In this appendix, we list the form factors of the one-loop corrections in Fig. 1. We give only the form factors of the decay $\tilde{\chi}_i^+ \rightarrow \tilde{\chi}_l^0 W^+$, $\Lambda_{(+il)}^{L,R}$ and $\Pi_{(+il)}^{L,R}$. For that of the decay $\tilde{\chi}_i^- \rightarrow \tilde{\chi}_l^0 W^-$, $\Lambda_{(-il)}^{L,R}$ and $\Pi_{(-il)}^{L,R}$, can correspondingly be obtained by conjugating all the couplings in $\Lambda_{(+il)}^{L,R}$ and $\Pi_{(+il)}^{L,R}$. Corresponding to the four one-loop diagram contributions, the form factors $\Lambda_{(+il)}^{L,R}$ and $\Pi_{(+il)}^{L,R}$ (in the following we omit “(+)”) can be divided into four parts,

$$\begin{aligned} \Lambda_{il}^{L,R} &= \Lambda_{il}^{(1)L,R} + \Lambda_{il}^{(2)L,R} + \Lambda_{il}^{(3)L,R} + \Lambda_{il}^{(4)L,R}, \\ \Pi_{il}^{L,R} &= \Pi_{il}^{(1)L,R} + \Pi_{il}^{(2)L,R} + \Pi_{il}^{(3)L,R} + \Pi_{il}^{(4)L,R} \end{aligned} \quad (21)$$

with

$$\begin{aligned} \Lambda_{il}^{(1)L} &= \frac{3}{8\pi^2} \sum_{j,k} A_{ik}^L C_{lj}^{L*} F_{kj} C_{24}^{(1)}, \quad \Lambda_{il}^{(1)R} = \Lambda_{il}^{(1)L} \quad (L \leftrightarrow R), \\ \Lambda_{il}^{(2)L} &= \frac{3}{8\pi^2} \sum_{j,k} B_{ij}^{L*} D_{lk}^L F_{kj} C_{24}^{(2)}, \quad \Lambda_{il}^{(2)R} = \Lambda_{il}^{(2)L} \quad (L \leftrightarrow R), \\ \Lambda_{il}^{(3)L} &= \frac{3g}{16\sqrt{2}\pi^2} \sum_k \left\{ m_b m_{\tilde{\chi}_i^0} A_{ik}^L D_{lk}^{R*} C_{12}^{(3)} - m_t m_{\tilde{\chi}_i^+} A_{ik}^R D_{lk}^{L*} (C_0^{(3)} + C_{11}^{(3)}) \right. \\ &\quad \left. + A_{ik}^L D_{lk}^{L*} \left[\frac{1}{2} + 2C_{24}^{(3)} + m_{\tilde{\chi}_i^+}^2 (C_{11}^{(3)} - C_{12}^{(3)} + C_{21}^{(3)} - C_{23}^{(3)}) \right] \right. \\ &\quad \left. + m_{\tilde{\chi}_i^0}^2 (C_{22}^{(3)} - C_{23}^{(3)}) + m_W^2 (C_{12}^{(3)} + C_{23}^{(3)}) \right\}, \end{aligned}$$

$$\begin{aligned}
\Lambda_{il}^{(3)R} &= \frac{3g}{16\sqrt{2}\pi^2} \sum_k \left\{ -m_t m_b A_{ik}^R D_{lk}^{R*} C_0^{(3)} + m_b m_{\tilde{\chi}_i^+} A_{ik}^L D_{lk}^{R*} C_{11}^{(3)} \right. \\
&\quad \left. - m_t m_{\tilde{\chi}_i^0} A_{ik}^R D_{lk}^{L*} (C_0^{(3)} + C_{12}^{(3)}) + m_{\tilde{\chi}_i^+} m_{\tilde{\chi}_i^0} A_{ik}^L D_{lk}^{L*} (C_{11}^{(3)} - C_{12}^{(3)}) \right\}, \\
\Lambda_{il}^{(4)L,R} &= \Lambda_{il}^{(3)L,R} \left(A_{ik}^{L,R} \leftrightarrow C_{lk}^{L,R}, D_{lk}^{L,R} \leftrightarrow B_{ik}^{L,R}, m_{\tilde{\chi}_i^+} \leftrightarrow m_{\tilde{\chi}_i^0}, \right. \\
&\quad \left. C_{0,11,12,21,22,23,24}^{(3)} \leftrightarrow C_{0,11,12,21,22,23,24}^{(4)} \right), \\
\Pi_{il}^{(1)L} &= -\frac{3}{16\pi^2} \sum_{j,k} F_{kj} \left[m_t A_{ik}^L C_{lj}^{R*} (C_{11}^{(1)} - C_{12}^{(1)}) + m_{\tilde{\chi}_i^0} A_{ik}^L C_{lj}^{L*} (C_{22}^{(1)} - C_{23}^{(1)}) \right. \\
&\quad \left. + m_{\tilde{\chi}_i^+} A_{ik}^R C_{lj}^{R*} (C_{11}^{(1)} - C_{12}^{(1)} + C_{21}^{(1)} - C_{23}^{(1)}) \right], \\
\Pi_{il}^{(1)R} &= \Pi_{il}^{(1)L} (L \leftrightarrow R), \\
\Pi_{il}^{(2)L} &= -\frac{3}{16\pi^2} \sum_{j,k} F_{kj} \left[m_b B_{ij}^{R*} D_{lk}^L (C_{11}^{(2)} - C_{12}^{(2)}) + m_{\tilde{\chi}_i^+} B_{ij}^{L*} D_{lk}^L (C_{22}^{(2)} - C_{23}^{(2)}) \right. \\
&\quad \left. + m_{\tilde{\chi}_i^0} B_{ij}^{R*} D_{lk}^R (C_{11}^{(2)} - C_{12}^{(2)} + C_{21}^{(2)} - C_{23}^{(2)}) \right], \\
\Pi_{il}^{(2)R} &= \Pi_{il}^{(2)L} (L \leftrightarrow R), \\
\Pi_{il}^{(3)L} &= \frac{3g}{16\sqrt{2}\pi^2} \sum_k \left[m_b A_{ik}^L D_{lk}^{R*} C_{12}^{(3)} + m_{\tilde{\chi}_i^0} A_{ik}^L D_{lk}^{L*} (C_{22}^{(3)} - C_{23}^{(3)}) \right], \\
\Pi_{il}^{(3)R} &= \frac{3g}{16\sqrt{2}\pi^2} \sum_k \left[-m_t A_{ik}^R D_{lk}^{L*} (C_0^{(3)} + C_{11}^{(3)}) \right. \\
&\quad \left. + m_{\tilde{\chi}_i^+} A_{ik}^L D_{lk}^{L*} (C_{11}^{(3)} - C_{12}^{(3)} + C_{21}^{(3)} - C_{23}^{(3)}) \right], \\
\Pi_{il}^{(4)L,R} &= \Pi_{il}^{(3)L,R} \left(A_{ik}^{L,R} \leftrightarrow C_{lk}^{L,R}, D_{lk}^{L,R} \leftrightarrow B_{ik}^{L,R}, m_{\tilde{\chi}_i^+} \leftrightarrow m_{\tilde{\chi}_i^0}, \right. \\
&\quad \left. C_{0,11,12,21,22,23}^{(3)} \leftrightarrow C_{0,11,12,21,22,23}^{(4)} \right), \tag{22}
\end{aligned}$$

where

$$\begin{aligned}
C_{11,12,21,22,23,24}^{(1)} &= C_{11,12,21,22,23,24}(m_{\tilde{\chi}_i^0}^2, m_{\tilde{\chi}_i^+}^2, m_W^2, m_{\tilde{t}_j}^2, m_t^2, m_{\tilde{b}_k}^2), \\
C_{11,12,21,22,23,24}^{(2)} &= C_{11,12,21,22,23,24}(m_{\tilde{\chi}_i^0}^2, m_{\tilde{\chi}_i^+}^2, m_W^2, m_{\tilde{b}_k}^2, m_b^2, m_{\tilde{t}_j}^2), \\
C_{0,11,12,21,22,23,24}^{(3)} &= C_{0,11,12,21,22,23,24}(m_{\tilde{\chi}_i^0}^2, m_{\tilde{\chi}_i^+}^2, m_W^2, m_b^2, m_{\tilde{b}_k}^2, m_t^2), \\
C_{0,11,12,21,22,23,24}^{(4)} &= C_{0,11,12,21,22,23,24}(m_{\tilde{\chi}_i^0}^2, m_{\tilde{\chi}_i^+}^2, m_W^2, m_t^2, m_{\tilde{t}_j}^2, m_b^2). \tag{23}
\end{aligned}$$

The definitions and numerical calculation formulae of the Passarino-Veltman one-, two-, and three-point functions are adopted from Refs [16].

References

- [1] H. P. Nilles, Phys. Rep. 110, 1 (1984); H. Haber and G. Kane, *ibid.* 117, 75 (1985).
- [2] M. Drees, hep-ph/9611409; S. P. Martin, hep-ph/9709356; M. Peskin, hep-ph/9705479; D. I. Kazakov, hep-ph/0012288.
- [3] S. Dimopoulos and D. Sutter, Nucl. Phys. B452, 496 (1996).
- [4] A. Masier and O. Vives, Nucl. Phys. B (Proc.Suppl.) 101, 253 (2001); T. Ibrahim and P. Nath, hep-ph/0107325.
- [5] I. S. Altarev *et al.*, Phys. Lett. B 276, 242 (1992); Y. Kizukuri, N. Oshimo, Phys. Rev. D 46, 3025 (1992); R. Garisto and J. D. Wells, Phys. Rev. D 55, 1611 (1997)
- [6] A. Pilaftsis, Phys. Lett. B 435, 88 (1998); D. A. Demir, Phys. Rev. D 60, 055006 (1999); M. Carena, J. Ellis, A. Pilaftsis, and C. E. M. Wagner, Nucl. Phys. B586, 92 (2000);
- [7] E. Christova, H. Eberl, S. Kraml and W. Majerotto, Nucl. Phys. B639, 263 (2002); W. M. Yang and D. S. Du, Phys. Rev. D 65, 115005 (2002).
- [8] M. Carena, J. M. Moreno, M. Quiros, M. Seco, and C. E. Wagner, Nucl. Phys. B599, 158 (2001); T. Ibrahim and P. Nath, Phys. Lett. B 418, 98 (1998); M. Brhlik, G. J. Good, and G. L. Kane, Phys. Rev. D 63, 035002 (2001).
- [9] T. Falk and K. V. Olive, Phys. Lett. B 439, 71 (1998); M. Carena, M. Quiros and C. E. Wagner, Nucl. Phys. B524, 3 (1998).
- [10] M. P. Worah, Phys. Rev. Lett. 79, 3810 (1997); N. Rius and V. Sanz, Nucl. Phys. B570, 1555 (2000); J. M. Cline, M. Joyce and K. Kainulainen, J. High Energy Phys. 07, 018 (2000).
- [11] J. F. Gunion and H. E. Haber, Phys. Rev. D 37, 2515 (1988); A. Djouadi, Y. Mambrini and M. Muhlleitner, Eur. Phys. J. C 20, 563 (2001); J. L. Feng and M. J. Strassler, Phys. Rev. D 55, 1326 (1997).
- [12] D. Atwood, S. Bar-Shalom, G. Eilam and A. Soni, Phys. Rep. 347, 1 (2001).
- [13] K. Hagiwara *et al.*, *Review of Particle Physics*, Phys. Rev. D 66, 1 (2002).

- [14] R. D. Heuer, D. J. Miller, F. Richard, and P. Zerwas, hep-ph/0106315; ECFA/DESY LC Physics Working Group Collaboration, E. Accomando *et al.*, Phys. Rep. 299, 1 (1998).
- [15] S. Kiyoura, M. M. Nojiri, D. M. Pierce and Y. Yamada, Phys. Rev. D 58, 075002 (1998).
- [16] G. Passarino and M. Veltman, Nucl. Phys. B160, 151 (1979); B. A. Kniehl, Phys. Rep. 240, 211 (1994).